Silver Film Growth on Glass Ceramic by Radio Frequency Magnetron Sputtering

Han Chao(韩超), *Xu Longxiang*(徐龙祥)*, *Ji Li*(纪历)

College of Mechanical and Electrical Engineering, Nanjing University of Aeronautics and Astronautics, Nanjing, 210016, P. R. China

(Received 27 Febuary 2013; revised 5 November 2013; accepted 8 November 2013)

Abstract: Thin silver films are deposited by radio frequency magnetron sputtering on glass ceramic at room temperature. Variations of sputtering power, bios voltage and power density are carried out for each deposition, then parts of as-deposited samples are subjected to annealing at 600 ℃ within a vacuum chamber. Structural properties are studied by X-ray diffraction (XRD), scanning electron microscope (SEM) and laser scanning confocal microscope (LSCM). It is shown that structural properties have a strong dependency on sputtering power and annealing temperature. Electrical contact resistance measured by a four point probe instrument is directly affected by the thickness of films. It is also found that the film conductivity, especially in thinner films, is improved by the increasing grain size. Finally, the film adhesion is observed by scratch tests. And the adhesive ability deposited by radio frequency magnetron sputtering shows a better performance than that produced by traditional methods.

Key words: silver; magnetron sputtering; glass ceramic; structural properties; contact resistance; adhesion force

CLC number: TB430.1 **Document code**: A **Article ID**: 1005-1120(2014)06-0629-07

1 Introduction

Metal films are widely used as coatings in the field of electronics, mainly because their low resistivity, high-thermal conductivity and excellent ductility[1,2]. Their properties have been extensively studied, but few researches have been offered to the application of metal films in high temperature. Traditionally, some active metals (Cr, Cu, Ni) are used for coating films. But they are easily contaminated by oxygen in high temperature. On the contrary, some inert metals (Au, Pt) which show strong stability in high temperature are difficult to obtain[3]. Finally, considering about the performance in inertness and cost-effective, silver attracts specific interest of researchers in coating films.

Different technologies have been reported to produce silver films with adequate performances for application in electronic devices: Physical vapor deposition (PVD), vacuum evaporation, vacuum winding coating, direct current (DC) and radio frequency (RF) magnetron sputtering[4]. In the work, silver films are prepared by RF magnetron sputtering for its some advantages: High deposition rate, high power efficiency, low temperature and good performances in smoothness, uniformity and binding force.

The use of glass ceramic disks as substrates for deposition has several advantages: Machinability makes it can be machined to be any shape, high temperature resistance makes it can be worked in high temperature environment and high thermal expansion coefficient (8.7×10^{-6}/℃) generates small thermal stress between silver films and substrates under large temperature difference[5,6].

2 Experiment

During the magnetron sputtering deposition,

Foundation item: Supported by the National Natural Science Foundation of China (50975134).

* **Corresponding author**: Xu Longxiang, Professor, E-mail: fqp@nuaa.edu.cn.

the circular sputtering target with 60 mm diameter composed of 99.99% purity pure silver is adopted, while the machinable glass ceramic (MGC) disks with 3 mm thickness and 10 mm diameter are chosen to be the substrates. Considering the bond strength between silver films and substrates, the glass ceramic disks are slightly polished to the roughness Ra of 1 μm.

All the substrates are cleaned in an ultrasonic bath with acetone and dried before inserted into vacuum chamber. The distance between target and substrate is 50 mm. The working pressure in vacuum chamber reach approximately 0.001 Pa due to the utilization of a turbo molecular-diaphragm pump combination.

The sputtering gas is filled with high-purity argon (99.99%) and the pressure is stably about 4 Pa. A gas flow controller is used to maintain the argon flow in the chamber at 10 standard-state cubic centimeter per minute (SCCM).

Before film deposition, the target is pre-sputtered on the shield about 30 min to remove the contaminations in the target surface and stabilize the magnetron parameters. In the deposition, the performances of the silver films are determined by the magnetron parameters, such as the sputtering power, bias voltage, power density, deposition rate, deposition time, deposition thickness, annealing condition, and so on. Therefore, the eight samples are distributed into four groups based on various magnetron parameters (as shown in Table 1).

Table 1 Samples with different processing parameters

Sample	Sputtering power/W	Bias voltage/V	Power density/ ($W \cdot cm^{-2}$)	Deposition rate/ ($nm \cdot min^{-2}$)	Deposition time/min	Deposition thickness/μm	Annealing condition
a_1	40	340	1.42	37	40	1.5	
a_2							Annealed
b_1	100	525	3.54	50	40	2	
b_2							Annealed
c_1	160	650	5.66	63	40	2.5	
c_2							Annealed
d_1	250	820	8.85	125	40	5	
d_2							Annealed

The samples (a_2, b_2, c_2, d_2) we chose from each group are placed into a vacuum chamber which is then pumped to a pressure of 1.3×10^{-3} Pa and annealed stepwise at temperature of 600 ℃ to anneal with 30 min. After cooling to room temperature, the chemical composition and crystal structure of all the films are analyzed by X-ray diffraction (XRD) D8 ADVANCE with Cu K α radiation and parallel beam geometry with a 2° incidence angle. And the surface morphologies of the films are observed by scanning electron microscope (SEM) JSM-6360LV JEOL. The surface roughness of the films is measured by a non-contact system named laser scanning confocal microscope (LSCM) OSL4000 OLYPUS. After that, the samples are cut apart and inlaid. Then, the inlaid samples are polished in order to observe the cross-section surface profile.

Moreover, the cross-section morphologies are observed by SEM. Considering the non-conductivity of cross-section, the inlaid samples are coated with 20 nm gold in 4 min by sputter coater K550X EMITECH in order to increase their conductivity.

Electrical resistivity of silver films is acquired at room temperature by four point probe instrument RG-7C from NAPSON Corporation. The thickness of films is also input into the four point probe instrument to ensure the accuracy. The contact force between probes and samples is detected and adjusted during measurement to avoid that the probes puncture thin films. This analysis delivers ρ values within an error margin of about 1%.

Finally, the film adhesion is measured by a micro scratch tester WS-2005. It is equipped with a standard diamond indenter with 120° taper angle and 0.2 mm radius. During the measurement, a loading rate of 25 N/min is used with scratches rate of 1 mm/min. In order to calculate the adhesive stress, the critical load is detected by a force sensor within the micro scratch tester in rupture position of films, thereafter the scratches images are observed by SEM.

3 Results and Analyses

3.1 X-ray diffraction

Fig. 1 shows the XRD spectrums of the silver films for the various different sputtering powers and annealing conditions. In order to minimize the errors of the experiment, prior to the analysis of the XRD spectrums, the back ground is subtracted. After this process, the diffraction peaks are completely symmetric and without any background. As shown in Fig. 1, the peaks indicate the polycrystalline nature of the silver films. And the strongest diffraction in each sample is the Ag (111), which can be observed in each sample. In addition, the peak becomes sharper with the increasing of sputtering power, meanwhile the splitting of diffraction peaks decrease or even disappear. Furthermore, the full-width at half-maximum (FWHM) of diffraction peak (111), micro-strain and crystallinity can be calculated by Jade 5.0 as shown in Table 2.

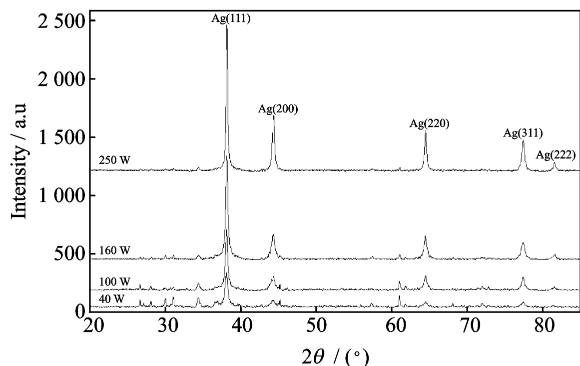

(a) As-deposited silver films with different sputtering power

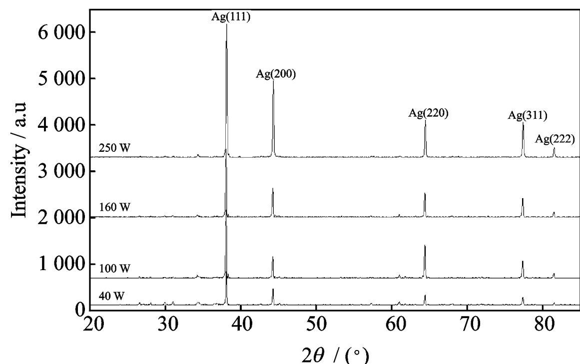

(b) Annealed silver films with different sputtering power

Fig. 1 XRD patterns for different silver films

Table 2 X-ray diffraction records of different samples

Sample	FWHM/(°)	Micro-strain/%	Crystallinity/%
a_1	0.435	0.185	57.86
a_2	0.145	0.081	60.84
b_1	0.335	0.226	54.33
b_2	0.133	0.073	58.95
c_1	0.280	0.230	52.23
c_2	0.138	0.080	58.59
d_1	0.213	0.211	50.58
d_2	0.132	0.077	58.27

Table 2 indicates that the crystallinity of as-deposited silver films decrease from 57.86% to 50.58% with the increasing of sputtering power, and the crystallinity silver films maintain at about 60% after annealed.

It confirms that lower growth rate causes the better crystalline quality of silver films, but the decrease of crystallinity is due to the less nucleation time of silver films at higher sputtering power. Meanwhile, the silver atoms at amorphous state have more free energy than that at crystalline state; annealing treatment gives silver films at amorphous state enough kinetic energy to transform into crystalline state by releasing free energy. Therefore, annealing treatment can improve their crystallinity[7].

The data of micro-strain express the degree of lattice distortion and crystal defect. As shown in Table 2, the micro-strain of as-deposited and annealed silver films are about 0.2% and 0.08%, respectively. The results show that the process of annealing treatment will reduce the degree of lattice distortion and crystal defect.

From the FWHM of diffraction peak (111), the average grain diameter of silver films can be estimated by the Scherrer formula as[8]

$$d=\frac{k\lambda}{\beta\cos\theta} \tag{1}$$

where d is the grain size in the silver films, the Scherrer constant k taken as 0.9, λ (0.154 06 nm) the wavelength of the X-ray, β the FWHM of peak (111) can be indicated from Table 2, and θ ($2\theta=38.2°$) the diffraction angle of peak (111).

Fig. 2 shows that the grain size of films is increased from 19.4 nm to 39.5 nm with the sputtering power increasing. With a higher growth rate, the initial silver crystals enlarge quickly before the nuclei are uniformly formed. The grain sizes become larger after annealing due to the merging processes[8].

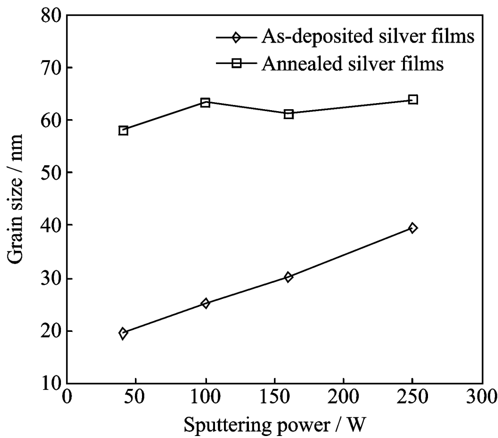

Fig. 2 Grain size of silver films with different sputtering power and different annealing condition

3.2 Microstructure

The influents both from the sputtering power and annealing condition are investigated by SEM measurement as shown in Fig. 3. In Figs. 3(a_1, a_2), the silver films at the lowest sputtering power show darker images than others due to the poor conductivity made by discontinuity of silver films in lower thickness.

With the increasing of sputtering power, continuous silver films are ultimately formed and the conductivity of films is strengthened. With the further increasing of sputtering power, one may notice that the value of surface roughness is significantly increased and more irregular protrusions are found (see Figs. 3(b_1—d_1)). Compared with as-deposited silver films image, smooth and continuous surface are found on every annealed film image (see Figs. 3 (a_2—d_2)). The possible reason is that the coalescence of silver atoms enlarges the average grain size of silver films calculated by Eq. (1) under the process of annealing treatment[3,9,10].

Fig. 4 shows cross-sectional SEM images of two silver films with the same sputtering power but different annealing condition. These two images show that the annealing process induces some changes in the morphological features of silver films. From the cross-section images with higher magnification (right columns of Figs. 4(a,b)), it can be clearly observed that silver aggregates have a significant change in size and shape, with diameters of grain varying from a few nanometers (see Fig. 4(a)) to about 60 nm (see Fig. 4(b)).

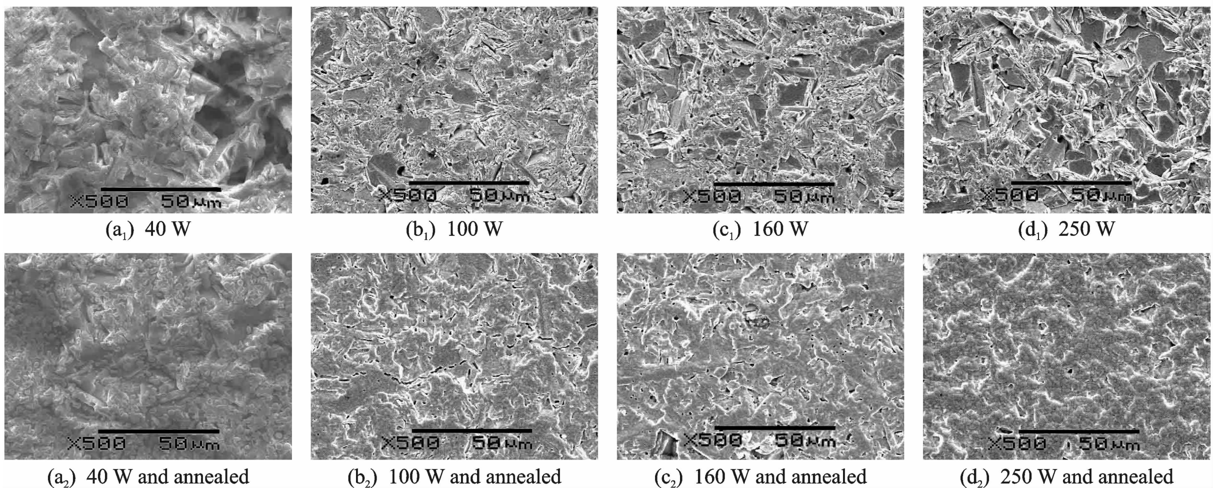

Fig. 3 Surface SEM images of silver films with different sputtering power and annealing condition

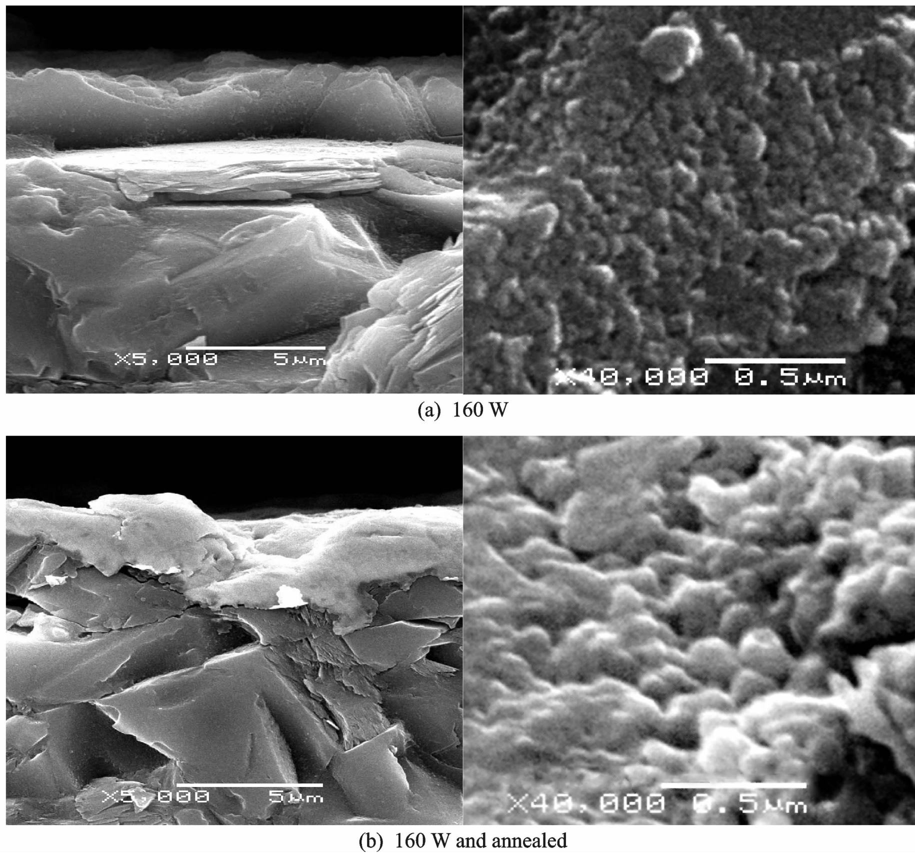

Fig. 4 Fractured cross-section SEM images of two silver films with different annealing condition

According to the theory proposed by K Heinemann and H Poppa[11], where the Ostwald ripening and short distance cluster mobility will appear simultaneously during the annealing of silver films onto MGC surfaces in the temperature about 600 °C, the experimental results can be explained. And this is confirmed by the variation of grain size detected by XRD shown in Fig. 2.

3.3 Electrical properties

The electrical resistivity of the different films at room temperature is measured by four probe measurements. The numerical value ρ_0 showed in instrument is calculated by the following equation[12]

$$\rho_0 = 2\pi S \frac{V}{I} \tag{2}$$

where S is the distance between two adjacent probes, V the potential difference between two inside probes, and I the current flowing thought two outside probes. ρ_0 can be considered to be electrical resistivity ρ theoretically, if the distance between test point and border of films is greater than $4S$. In the experiment, the condition of distance is not met. Therefore, the modifying factor B_0 should be taken in consideration, and electrical resistivity ρ should be written as

$$\rho = \frac{\rho_0}{B_0} = 2\pi S \frac{V}{I} \cdot \frac{1}{B_0} \tag{3}$$

The electrical resistivity ρ of silver films with different thickness and annealing condition after correction is showed in Fig. 5.

In Fig. 5, it can be noticed that silver films of 1.5 μm thickness exhibit higher resistance (about 200 μΩ · cm) than that of others. This can explain the fact that the silver films at the lowest sputtering power exhibit darker images which showed in Fig. 3. When the film thickness increases to 2 μm, the ρ value decreases dramatically to about 40 μΩ · cm. When the film thickness further increases about 5 μm, the ρ value reaches about 3 μΩ · cm, being almost the same as that of bulk Ag (1.6 μΩ · cm). And with increasing of deposition thickness, the non-uniformity of resistivity decreases from 10% at 1.5 μm to 4% at 5 μm. Therefore, a conclusion can be made that

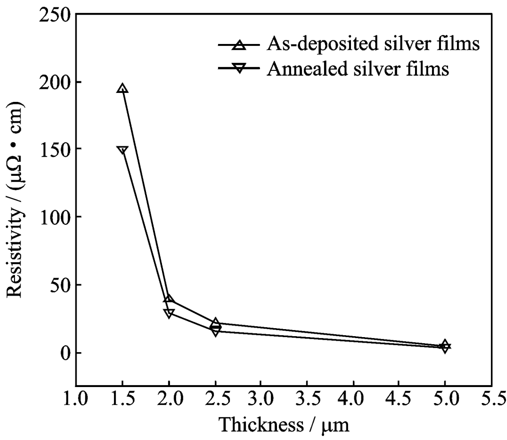

Fig. 5 Variation of electrical resistivity with different film thickness and annealing condition

the electrical resistivity is directly affected by the thickness of films.

One may also notice that, the ρ value of silver films at thickness of 1.5 μm is lower after the annealing treatment than they have been before it, falling from 196 $\mu\Omega \cdot$ cm to 150 $\mu\Omega \cdot$ cm, because the increasing crystal grain size caused by annealing treatment decreases the grain boundary scattering of electrons[9,13].

3.4 Scratch tests

Scratch tests of silver films are carried out for with a loading rate of 25 N/min. Fig. 6(a) shows the total scratch track of film for an increasing load from 0 to 100 N in 4 min. The width of scratch track is obviously broadened with the increasing of load[14]. When the contact force reaches to the critical load, the delaminating between film and substrate occurs, and the scratch track at the rupture position is shown in Fig. 6(b).

The critical load for all films shows the similar value about 30 N. It can be deduced that what directly affects the critical load are not the film thickness and annealing condition but the property of substrate and coating technique.

Fig. 7 shows the relationship between force and deformation of film in the scratch tests. Where r is the radius of indenter with 0.2 mm, W the contact force given by indenter, d the width of scratch track which can be measured from Fig. 6, P the resistance given by substrate

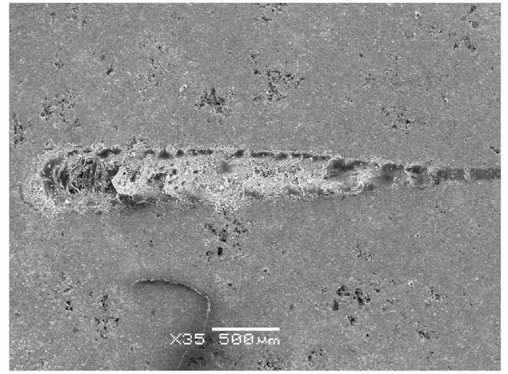

(a) Scratch track of film with an increasing load from 0 to 100 N

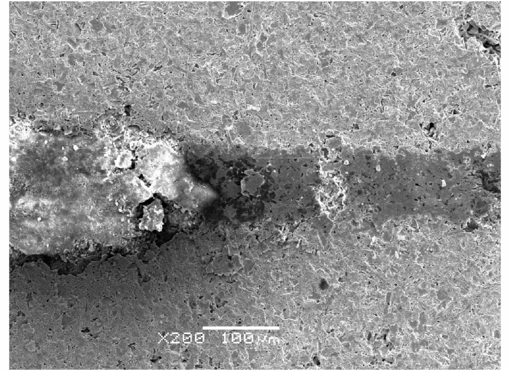

(b) Scratch track of film in rupture position

Fig. 6 SEM images of scratch tests for silver films

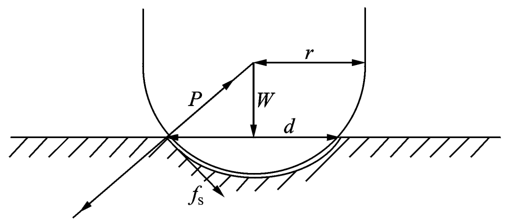

Fig. 7 Relationship between force and deformation of film

which can be expressed as[15]

$$P = \frac{W}{\pi d^2} \tag{4}$$

and f_S the shear press of film which can be calculated by the following equation

$$f_S = \sqrt{\frac{W}{\pi r^2 P - W}} \cdot P \tag{5}$$

When W equals to the critical load W_C, the critical value of f_S can be considered as the adhesive stress and it should be equal to

$$f_{SC} = \sqrt{\frac{W_C}{\pi r^2 P - W_C}} \cdot P \tag{6}$$

According to Eq. (6), the range of critical values (f_{SC}) is calculated to be 245 N/mm^2. Compared with the traditional methods such as electropla-

ting and directing bonding (80 N/mm^2)[16], the films deposited by RF magnetron sputtering shows a better performance due to the excellent penetrating power of high kinetic energy silver atoms.

4 Conclusions

Thin silver films are deposited on glass ceramic by RF magnetron sputtering at room temperature. As a result, the deposition rate rises from 50 nm/min to 125 nm/min with the increasing of the sputtering power.

After that, annealing treatments at 600 ℃ are carried out on parts of as-deposited samples. And the microstructure, the topography, the electrical properties and the adhesive stress of films are investigated by X-ray diffraction, scanning electron microscope, four point probe instrument and micro scratch tests, respectively.

The experimental results show that the increasing of sputtering power will increase the grain size as well as the surface roughness. In addition, due to the annealing treatments, the grain size further increases, whereas the surface roughness is dropped.

For thicker films (5 μm), deposition at 250 W led to a low value of the resistivity (3 $\mu\Omega \cdot cm$) compared with that of bulk Ag (1. 6 $\mu\Omega \cdot cm$). Annealing treatment reduces the resistivity due to the increasing of crystal grain size. However, the observed changes of conductivity are mainly attributed to differences in the film thickness and the surface topography. And the adhesive stress deposited by RF magnetron sputtering reaches 245 N/mm^2, which shows a significant improvement compared with traditional methods.

References:

[1] Suzuki T, Abe Y, Kawamura M, et al. Optical and electrical properties of pure Ag and Ag-based alloy thin films prepared by RF magnetron sputtering [J]. Vacuum, 2002, 66(3/4): 501-504.

[2] Sarakinos K, Wördenweber J, Uslu F, et al. The effect of the microstructure and the surface topography on the electrical properties of thin Ag films deposited by high power pulsed magnetron sputtering [J]. Surf Coat Technol, 2008, 202(11): 2323-2327.

[3] Adochite R C, Munteanu D, Torrell M, et al. The influence of annealing treaments on the properties of Ag: TiO_2 nanocomposite films prepared by magnetron sputtering[J]. Surf Sci, 2012, 258: 4028-4034.

[4] Kelly P G, Arnell R D. Magnetron sputtering: A review of recent developments and applications [J]. Vacuum, 2000, 56(3):159-172.

[5] Voss S, Gandikota S, Tao R, et al. Adhesion studies of CVD copper metallization [J]. Microelectronic Eng, 2000, 50(1/2/3/4):501-508.

[6] Iwase N, Tsuge A, Sugiura Y. Development of a thermal conductive AIN ceramic substrate technology [J]. Hybrid Microelectron, 1984, 7:49-53.

[7] Kapaklis V, Poulopoulos P, Karoutsos V, et al. Growth of thin Ag films produced by radio frequency magnetron sputtering [J]. Thin Solid Films, 2006, 510(1/2): 138-142.

[8] Duan L, Yu X, Ni L, et al. ZnO: Ag film growth on Si substrate with ZnO buffer layer by RF sputtering [J]. Appl Surf Sci, 2011, 257(8): 3463-3467.

[9] Sun Daming, Sun Zhaoqi. Metal ceramic film and its applications in photoelectron technology [M]. Beijing: Science Press, 2004. (in Chinese)

[10] Jiang Chuanhai, Yang Chuanzheng. Analysis of materials by ray-diffraction and scattering [M]. Beijing: Higher Education Press, 2010. (in Chinese)

[11] Heinemann K, Poppa H. Direct observation of small cluster mobility and ripening[J]. Thin Soild Films, 1976,33(2):237-251.

[12] Wang Huabi, Wu Ziqin. Advocating the physical experiment method [M]. Beijing: Higher Education Press, 1990. (in Chinese)

[13] Nedfors N, Tengstrand O, Lewin E, et al. Structural, mechanical and electrical-contact properties of nanocrystalline-NbC/amorphous-C coatings deposited by magnetron sputtering [J]. Surf Coat Technol, 2011, 206(2/3): 354-359.

[14] Senna L F, Achete C A, Hirsch T, et al. Structural, chemical, mechanical and corrosion resistance characterization of TiCN coatings prepared by magnetron sputtering [J]. Surf Coat Technol, 1997, 94/95: 390-397.

[15] Xiao Dingquan, Zhu Jianguo, Zhu Jiliang, et al. Film physics and device [M]. Beijing: National Defense Industry Press, 2011. (in Chinese)

[16] Jing M, Fu R L, He H, et al. Direct bonded metal substrates and bonding methods [J]. Aerospace Materials and Technology, 2008, 3:1-7.

(Executive editor: Xu Chengting)